Light inactivation of water transport and protein–protein interactions of aquaporin–Killer Red chimeras

Florian Baumgart,[1,2] Andrea Rossi,[1,2] and A.S. Verkman[1,2]

[1]Department of Medicine and [2]Department of Physiology, University of California, San Francisco, San Francisco, CA 94143

Aquaporins (AQPs) have a broad range of cellular and organ functions; however, nontoxic inhibitors of AQP water transport are not available. Here, we applied chromophore-assisted light inactivation (CALI) to inhibit the water permeability of AQP1, and of two AQP4 isoforms (M1 and M23), one of which (M23) forms aggregates at the cell plasma membrane. Chimeras containing Killer Red (KR) and AQPs were generated with linkers of different lengths. Osmotic water permeability of cells expressing KR/AQP chimeras was measured from osmotic swelling–induced dilution of cytoplasmic chloride, which was detected using a genetically encoded chloride-sensing fluorescent protein. KR-AQP1 red fluorescence was bleached rapidly (~10% per second) by wide-field epifluorescence microscopy. After KR bleaching, KR-AQP1 water permeability was reduced by up to 80% for the chimera with the shortest linker. Remarkably, CALI-induced reduction in AQP4-KR water permeability was approximately twice as efficient for the aggregate-forming M23 isoform; this suggests intermolecular CALI, which was confirmed by native gel electrophoresis on cells coexpressing M23-AQP4-KR and myc-tagged M23-AQP4. CALI also disrupted the interaction of AQP4 with a neuromyelitis optica autoantibody directed against an extracellular epitope on AQP4. CALI thus permits rapid, spatially targeted and irreversible reduction in AQP water permeability and interactions in live cells. Our data also support the utility of CALI to study protein–protein interactions as well as other membrane transporters and receptors.

The Journal of General Physiology

INTRODUCTION

Aquaporin (AQP) water channels are integral membrane proteins of ~30 kD molecular mass that consist of six membrane-spanning helical segments surrounding a narrow aqueous pore (Walz et al., 1994, 2009; Ho et al., 2009). AQPs are assembled in membranes as tetramers in which each monomer functions as an independent transport unit (Verbavatz et al., 1993; Shi et al., 1994). AQP-facilitated water transport is involved in many aspects of mammalian physiology, including transepithelial fluid transport, brain water balance, cell migration, and neuroexcitation (Verkman, 2008). AQPs are important as well in invertebrates, plants, yeast, and bacteria (Maurel, 2007; Soveral et al., 2010). A subset of the AQPs, called aquaglyceroporins, transport both water and glycerol, and are involved in fat metabolism, cell proliferation, and epidermal hydration (Rojek et al., 2008).

Much of the information about the biological functions of AQPs has come from phenotype studies on knockout mice lacking individual AQPs, in part because nontoxic inhibitors of AQP function are not available. The water/glycerol transport functions of some AQPs are inhibited by Hg^{2+} and other heavy metal ions by nonspecific sulfhydryl reaction (Preston et al., 1993; Zhang et al., 1993); however, heavy metal ions are too toxic for use in live cells. A few small-molecule AQP inhibitors have been described (Ma et al., 2004; Huber et al., 2009a,b); however, subsequent work has not confirmed their activity (Yang et al., 2006, 2008; Søgaard and Zeuthen, 2008). There is thus a need for approaches to rapidly and selectively reduce AQP water permeability in live cells and tissues. For example, rapid inactivation of water permeability in migrating cells would allow quantification of the water permeability dependence of lamellipodial dynamics, and hence clarify proposed cellular mechanisms of AQP-facilitated cell migration (Saadoun et al., 2005; Papadopoulos et al., 2008).

Here, we investigated the utility of chromophore-assisted light inactivation (CALI) to reduce AQP-facilitated water permeability in live cells. CALI relies on the localized generation of oxygen radicals by a fluorophore after light exposure. CALI has been used to abolish membrane targeting of lipid-interacting PH domains (Bulina et al., 2006), interfere with myosin-dependent cell polarization in whole *Drosophila* embryos (Monier et al., 2010), inhibit cell cycle progression (Serebrovskaya et al., 2011), and ablate specific cells in developing

Correspondence to Alan S. Verkman: Alan.Verkman@ucsf.edu

Abbreviations used in this paper: AQP, aquaporin; BN/PAGE, Blue-native PAGE; CALI, chromophore-assisted light inactivation; FRT, Fisher rat thyroid; KR, Killer Red; NMO, neuromyelitis optica; OAP, orthogonal array of particle; ROS, reactive oxygen species; SE, standard error; TIRFM, total internal reflection fluorescence microscopy.

The Rockefeller University Press $30.00
J. Gen. Physiol. Vol. 139 No. 1 83–90
www.jgp.org/cgi/doi/10.1085/jgp.201110712

zebrafish embryos (Del Bene et al., 2010). Based on our successful use of fluorescent protein–AQP chimeras for a variety of studies on AQP targeting, function, diffusion, and membrane assembly (Umenishi et al., 2000; Levin et al., 2001; Tajima et al., 2010), we generated chimeras of AQPs 1 and 4 with Killer Red (KR), a genetically encoded protein with efficient photosensitizing activity (Bulina et al., 2006). We demonstrate CALI-mediated inhibition of osmotic water permeability in live cells and investigate the intra- and intermolecular determinants of CALI efficiency. In addition to the utility of CALI for rapid and irreversible inhibition of cell membrane water permeability, we provide evidence for application of CALI for investigation of protein–protein interactions.

MATERIALS AND METHODS

DNA constructs

pKillerRed-C was purchased from Evrogen. Human AQP1 and AQP4 sequences were PCR-amplified from pcDNA3.1-AQP1 and AQP4, respectively. KR was appended at the N terminus of the AQP1 sequence as follows (Fig. 1): KR-AQP1 long was generated using KpnI and ApaI restriction sites, in which a 17–amino acid linker separates KR and AQP1. KR-AQP1 was generated using BspEI and BamHI sites, giving a 3–amino acid linker. KR-AQP1 short, which was generated by PCR, contains AQP1 at the C terminus of KR in which the seven C-terminal amino acids were deleted. We also created a chimera with KR at the C terminus of AQP1 (AQP1-KR). KR was appended at the C terminus of AQP4 sequences. Membrane-targeted KR (KRmem) was generated by ligating a duplex of complimentary oligonucleotides encoding the C-terminal 12 amino acids of H-Ras (GPGCMSCKCVLS) in frame with the KR sequence. M23-AQP4 containing an extracellular myc tag has been described previously (Crane and Verkman, 2009). All constructs were verified by sequence analysis.

Cell culture and transfection

Fisher rat thyroid (FRT) cells (American Type Culture Collection CRL-1468) were cultured in Coon's modified F-12 medium (Sigma-Aldrich) supplemented with 10% fetal bovine serum, 2 mM glutamine, 100 U/ml penicillin, and 100 µg/ml streptomycin. U87MG cells (human glioblastoma-astrocytoma, American Type Culture Collection HTB-14) were cultured in DME supplemented with 10% fetal bovine serum, 2 mM glutamine, 100 U/ml penicillin, and 100 µg/ml streptomycin. Cells were maintained at 37°C in 5% CO_2/95% air. For CALI, cells were seeded on glass coverslips and transfected with the respective DNA constructs in antibiotic-free medium 12–24 h before experiments using Lipofectamine 2000 (Invitrogen) according to the manufacturer's instructions.

Osmotic water permeability

Osmotic water permeability was measured from the kinetics of cell swelling after rapid reduction in extracellular osmolality from 300 to 150 mOsm. Cell swelling causes instantaneous dilution of cytoplasmic chloride, which was detected from the fluorescence of the genetically encoded fluorescent protein, YFP-H148Q/V163S (Galietta et al., 2001). Cells expressing YFP-F148Q/V163S alone or together with an AQP/KR chimera were mounted in a custom perfusion chamber. YFP-H148Q/V163S fluorescence was recorded at 2 Hz for 60 s using an inverted epifluorescence microscope (TE200S; Nikon) equipped with a 40× objective lens and an FITC filter set. Single-cell fluorescence was quantified using Fiji software (http://fiji.sc/wiki/index.php/Fiji). After background subtraction, YFP fluorescence versus time was fitted to a single exponential function to give the exponential time constant τ. Percentage inhibition was computed as: % inhibition = 100 $[1 - (\tau^{-1}_{CALI} - \tau^{-1}_{b})/(\tau^{-1}_{0} - \tau^{-1}_{b})]$, where τ^{-1}_{0} is the water transport rate in cells outside the bleached area, τ^{-1}_{CALI} is the rate in bleached cells, and the τ^{-1}_{b} is the baseline, AQP-independent water transport rate measured in FRT cells expressing YFP alone.

Light inactivation

For CALI, KR fluorescence was bleached for specified times using a TR/Cy3.5 filter cube (540–580 nm transmitted light at 18 mW/cm^2; Chroma Technology Corp.) through a 100× oil-immersion objective lens (numerical aperture 1.4; Nikon), which bleached a 175-µm-diameter circular area. After bleaching, osmotic water permeability was measured as described in the previous paragraph.

Cell viability assay

Cell viability after CALI was determined using SYTOX green (Invitrogen). After CALI as described in the previous paragraph, cells were incubated for 10 min with 5 µM SYTOX green in PBS. As a positive control, cells were incubated for 10 min with 0.3% Triton X-100 before SYTOX green staining.

Gel electrophoresis and immunoblot analysis

SDS/PAGE was done using NuPAGE 4–12% Bis-Tris precast gels (Invitrogen). Proteins were blotted onto polyvinylidene difluoride (PVDF) membranes (Millipore) in NuPAGE transfer buffer. AQP1, AQP4, and myc-epitope tagged AQP4 were immunodetected using polyclonal antibodies (Santa Cruz Biotechnology, Inc.). Blue-native PAGE (BN/PAGE) was performed as described previously (Rossi et al., 2011).

CALI of cell homogenates

FRT cells were transfected with M1-AQP4-KR or M23-AQP4-KR, each together with unconjugated AQP1. In some experiments, FRT cells were transfected with M23-AQP4-KR together with M23-AQP4 containing an extracellular myc tag. At 24–28 h after transfection, cells were detached using trypsin, pelleted, and lysed in 50 µl of native buffer (500 mM ε-aminocaproic acid, 50 mM imidazole, pH 7.0, 12 mM NaCl, 10% glycerol, 1% Triton X-100, and protease inhibitor cocktail). The cell homogenate was transferred to a coverglass and subjected to CALI using a 561-nm argon ion laser to reduce KR fluorescence by >95%. Cell homogenates were analyzed by BN/PAGE and immunoblotted with anti-AQP4, anti-AQP1, and/or anti-myc antibodies.

Total internal reflection fluorescence microscopy (TIRFM)

TIRFM was done using a microscope (Eclipse TE2000E; Nikon) equipped with a through-objective TIRF attachment and a 100× oil immersion objective lens (numerical aperture 1.49). M23-AQP4-GFP and M23-AQP4-KR fluorescence were excited using an argon ion laser and appropriate filter sets. Images were acquired using a deep-cooled charge-coupled device camera (QuantEM 512SC; Photometrics).

Neuromyelitis optica (NMO)-IgG binding

NMO serum was obtained from an NMO-IgG seropositive patient. Purified IgG from NMO serum was isolated using a Melon Gel IgG Spin Purification kit (Thermo Fisher Scientific). U87MG cells transfected with M23-AQP4-KR or M23-AQP4 + cytoplasmic KR (as control) were incubated in blocking buffer (PBS containing 6 mM glucose, 1 mM pyruvate, and 1% BSA) for 20 min followed by 30 min of incubation with purified NMO-IgG (1:100 dilution in blocking buffer). Cells were

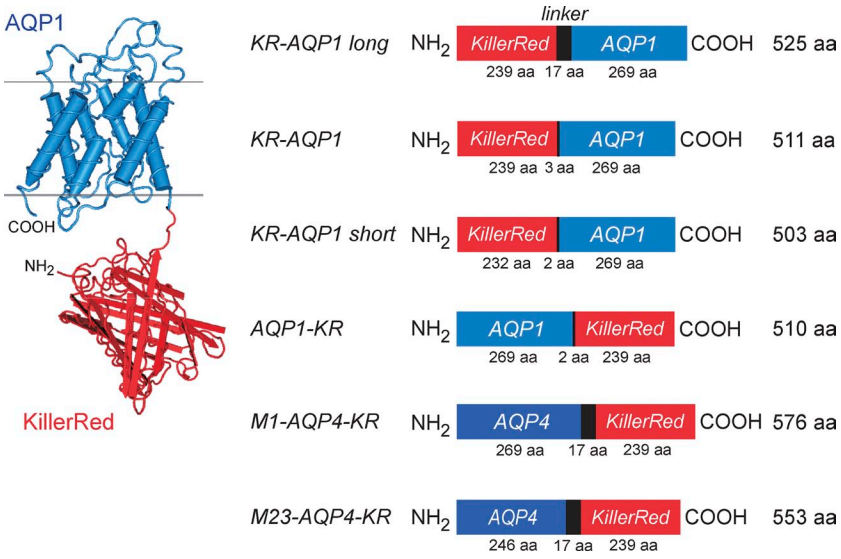

Figure 1. KR/AQP chimeras. (left) Schematic of a KR/AQP1 chimera with KR at the AQP1 N terminus. (right) Chimeras generated for CALI studies, including three AQP1 N-terminal chimeras of different lengths. Linkers of 17 and 3 amino acids separated KR and full-length AQP1 in KR-AQP1 long and KR-AQP1, respectively. In KR-AQP1 short, the seven C-terminal amino acids of KR were truncated. AQP1-KR and AQP4-KR (M1 and M23) were generated as C-terminal chimeras.

then rinsed with PBS three times and labeled with Alexa Fluor 488–conjugated goat anti–human secondary antibodies (1:1,000 dilution in blocking buffer; Invitrogen). CALI was performed as described in the previous paragraph. Images were analyzed to compute area-integrated, background-subtracted Alexa Fluor 484 fluorescence within and outside of the KR bleached area.

RESULTS

To apply CALI for spatially targeted inactivation of AQP-mediated water transport in live cells, chimeras were generated consisting of KR and AQPs 1 or 4 (Fig. 1). KR is a genetically encoded photosensitizer. Light inactivation by KR is thought to involve the local generation of reactive oxygen species (ROS) and consequent damage to nearby proteins (Liao et al., 1994). AQP1 assembles at the cell plasma membrane in tetramers (Verbavatz et al., 1993), where it freely diffuses (Crane and Verkman, 2008). KR was appended to the N terminus of AQP1 because of its shorter length compared with the AQP1 C terminus and because N-terminal GFP-AQP1 chimeras were found previously to be functional and efficiently processed (Umenishi et al., 2000). Linkers of different lengths connecting KR and AQP1 were tested. We also generated an AQP1-KR chimera with KR appended at the AQP1 C terminus.

AQP4 is another water-selective transporter, which is expressed in two isoforms produced by alternative splicing: a long isoform with translational initiation at Met-1 (M1-AQP4) and a short isoform with translation initiation at Met-23 (M23; Yang et al., 1995; Lu et al., 1996). M1-AQP4 tetramers freely diffuse in the cell plasma membrane, whereas M23-AQP4 tetramers assemble in large, nearly immobile aggregates called orthogonal arrays of particles (OAPs; Yang et al., 1996; Verbavatz et al., 1997). Because N-terminal interactions are responsible for OAP formation by M23-AQP4 (Crane and Verkman, 2009), KR was appended to the AQP4 C terminus. AQP4-GFP chimeras were shown previously to be functional and processed efficiently (Tajima et al., 2010). These constructs allowed investigation of the intramolecular and intermolecular determinants of CALI inactivation of AQP water permeability.

Each of the chimeras was expressed in FRT cells, which were chosen for their low basal water permeability, absence of AQP expression, and efficient transfection. A new fluorescence method was developed to measure osmotic water permeability in transiently transfected cells expressing KR/AQP chimeras. The method uses a genetically encoded fluorescent chloride sensor (YFP-H148Q/V163S), which was developed previously by our laboratory (Galietta et al., 2001), to follow the kinetics of decreasing cytoplasmic chloride concentration that accompanies osmotically induced cell swelling. Cells were transfected with YFP alone or together with a KR/AQP chimera. The time course of YFP fluorescence was measured in response to a rapid, twofold dilution of the extracellular solution. For CALI, a small circular area was illuminated with red light using a high-magnification (100×) objective lens, which bleached KR but not YFP fluorescence (Fig. 2 A). Osmotic water permeability was then measured at lower magnification (40×) to enable visualization of cells that were exposed to the red light as well as nonexposed cells. KR bleaching was rapid, with 50% loss of red fluorescence in <10 s (Fig. 2 B). Cell viability was not affected by CALI as shown by vital dye exclusion (Fig. 2 C).

With SDS/PAGE and AQP1 immunoblotting, the KR/AQP1 chimeras expressed in FRT cells migrated at their appropriate molecular sizes, with no nonconjugated AQP1 seen (Fig. 3 A, top). For comparison, AQP1 (in kidney homogenate, left lane) and a GFP-AQP1

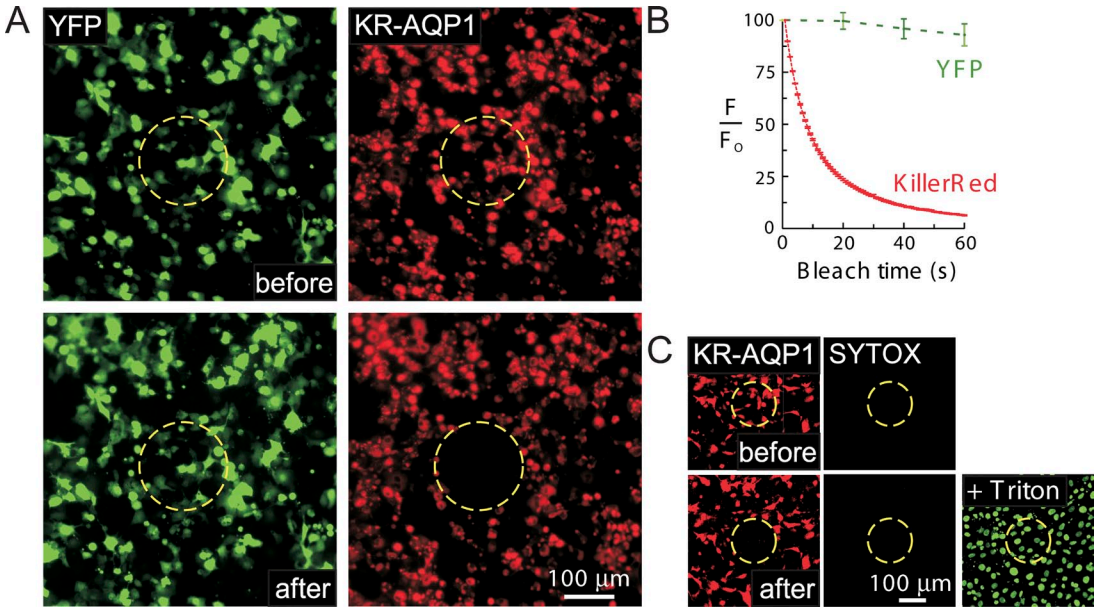

Figure 2. Photobleaching of KR-AQP1. (A) FRT cells coexpressing a YFP chloride sensor (green) and KR-AQP1 short (red) were imaged at 20× magnification before (top) and after (bottom) CALI (exposure to red light for 60 s) in the indicated circular regions (circles). (B) Fluorescence of YFP and KR during CALI (error bars indicate standard error [SE], $n = 4$). (C) Cell viability assayed after CALI (0.3% Triton X-100 as a positive control). Dead cells were stained green (SYTOX).

chimera (second lane) are shown. Fig. 3 A (bottom) demonstrates the YFP method for measurement of osmotic water permeability as applied to FRT cells expressing (nonconjugated) AQP1. After rapid reduction in extracellular osmolality, YFP fluorescence increased in an approximately exponential manner with a time constant of 1.5 ± 0.2 s.

Fig. 3 B shows slow osmotic cell swelling in control (non–AQP1-expressing) cells, which was much more rapid in cells expressing each of the three KR/AQP1 chimeras. Fig. 3 C summarizes osmotic swelling rates. Although CALI had little effect on water permeability of the KR/AQP1 construct with the longest linker (KR-AQP1 long), water permeability was reduced by 45% and 80% for KR-AQP1 and KR-AQP1 short, respectively. CALI of a C-terminal AQP1/KR chimera did not reduce water permeability, nor did CALI of cells coexpressing AQP1 and a membrane-targeted KR. CALI efficiency was measured as a function of the time of red light exposure. Fig. 3 D (top) shows lower water permeability with more prolonged red light exposure. The data summary in Fig. 3 D (bottom) indicates an approximately exponential reduction in osmotic water permeability with red light exposure time, with a maximum ∼80% reduction. The figure inset shows a nonlinear relationship between percentage water transport inhibition and percentage KR bleach, which suggests a cooperative mechanism in which more than one "hit" is required to produce inactivation.

CALI measurements were also done for KR/AQP4 chimeras. BN/PAGE, which has been used to resolve supramolecular AQP4 aggregates, shows the presence of aggregates in cells expressing M23-AQP4-KR but not M1-AQP4-KR (Fig. 4 A, left). TIFRM of the transfected cells confirmed aggregate/OAP formation by M23-AQP4-KR but not by M1-AQP4-KR (Fig. 4 A, right). Fig. 4 B shows representative data for osmotic cell swelling and Fig. 4 C summarizes swelling rates. Both M23-AQP4-KR and M1-AQP4-KR substantially increased osmotic water permeability compared with control (non–AQP4-expressing) cells. CALI resulted in 42% inhibition of water permeability of M1-AQP4-KR, compared with 75% for M23-AQP4-KR. The increased CALI efficiency for M23-AQP4-KR is likely the consequence of AQP4-M23 clustering in the plasma membrane and intermolecular CALI effects.

The enhanced CALI efficiency found for M23-AQP4 aggregates suggested to us the possibility of applying CALI to study protein–protein interactions. As a test example, CALI of AQP4-KR was done to attempt to disrupt the interaction of AQP4 with an anti-AQP4 antibody that binds to an extracellular AQP4 epitope (Fig. 5). This antibody has been implicated in the neuroinflammatory demyelinating disease NMO, in which antibody-AQP4 binding causes astrocyte damage in the central nervous system (Jarius and Wildemann, 2010). Purified NMO-IgG was bound to live U87MG cells expressing M23-AQP4-KR, or, as a control, unconjugated M23-AQP4 and cytoplasmic KR. Fig. 5 shows that after NMO antibody binding followed by labeling with an Alexa Fluor 488–labeled secondary antibody, CALI resulted in ∼70% reduction in NMO-IgG binding in

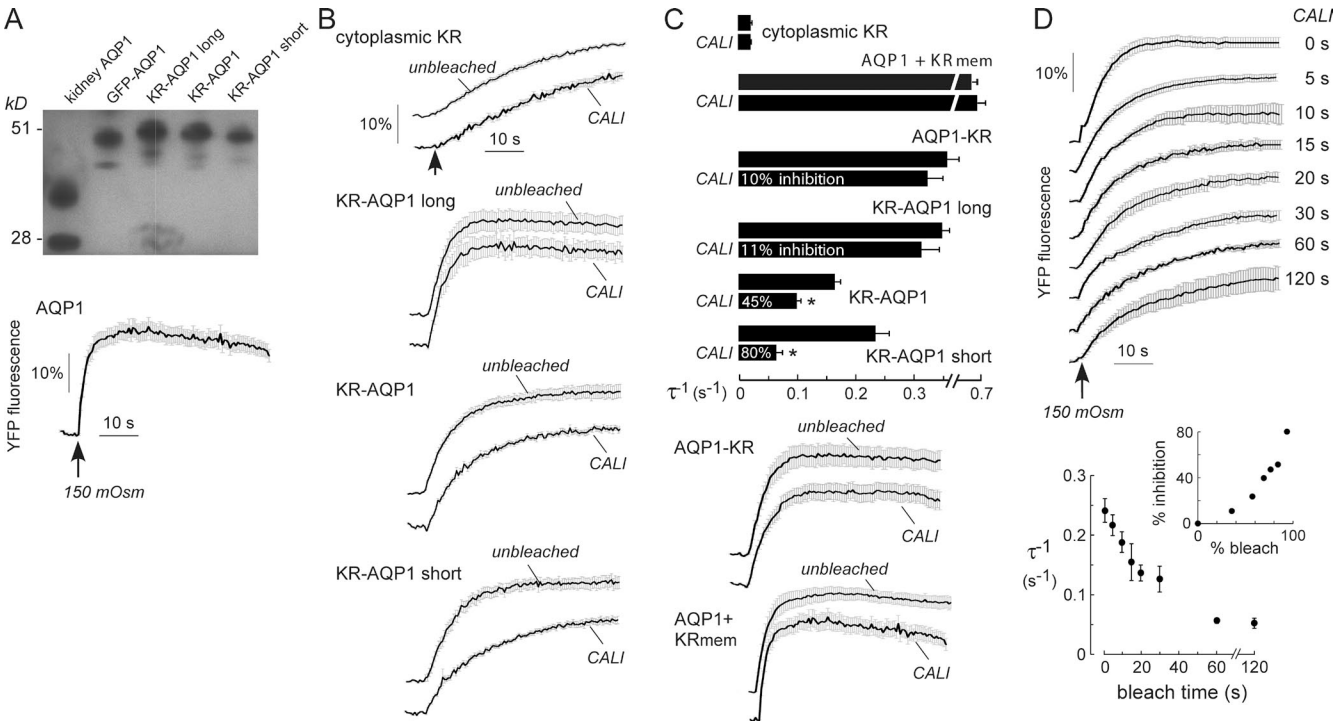

Figure 3. Reduced osmotic water permeability of KR/AQP1 chimeras after CALI. FRT cells were transfected with YFP alone or together with indicated KR/AQP1 chimeras. (A, top) AQP1 immunoblot after SDS/PAGE of cells expressing indicated KR/AQP1 chimeras. Also shown are AQP1 (in kidney lysate) and FRT cells expressing a GFP-AQP1 chimera. Gels that are apart were run separately. (A, bottom) Time course of YFP fluorescence in cells expressing AQP1 (without KR) after rapid reduction in osmolality of the extracellular solution from 300 to 150 mOsm. (B) Osmotic water permeability as in A (bottom) for FRT cells expressing YFP and KR in cytoplasm, KR targeted to the plasma membrane (KRmem), and indicated KR/AQP1 chimeras. (C) Summary of relative osmotic water permeabilities (expressed as reciprocal exponential time constant τ^{-1}) deduced from experiments in B ($n = 5$–8 cells on three cover glasses, error bars indicate SE; *, $P < 0.01$). (D) Dependence of AQP1 water permeability inactivation on KR bleaching for KR-AQP1 short. (D, top) Osmotic water permeability in cells exposed to CALI for the indicated times. (D, bottom) Relative water permeability versus CALI bleach time ($n = 5$–8 cells on three cover glasses, error bars indicate SE; *, $P < 0.01$). (D, inset) Percentage inhibition of water permeability versus percentage of KR bleach (reduction in fluorescence).

cells expressing M23-AQP4-KR in a circular spot preilluminated by the red light, whereas NMO-IgG binding to unconjugated M23-AQP4 was not reduced.

We postulated that the reduction in NMO-IgG binding to AQP4 after CALI was caused by generalized disruption of AQP4 structure. BN/PAGE was done on homogenates from FRT cells expressing M1-AQP4-KR or M23-AQP4-KR, each together with unconjugated AQP1 as a non–KR-conjugated bystander membrane protein. Fig. 6 A shows that CALI produced extensive alterations in the gel pattern of M1-AQP4-KR and M23-AQP4-KR, without effect on AQP1.

Last, to further investigate intermolecular CALI, cells were transfected with M23-AQP4-KR together with myc-tagged M23-AQP4, which are expected to co-assemble in OAPs. CALI performed on cell homogenates produced extensive alterations in the gel patterns of both proteins, as seen in AQP4 and myc immunoblots (Fig. 6 B). These data implicate intermolecular CALI, which suggests that ROS produced from light-exposed KR can affect nearby proteins.

DISCUSSION

We established the utility of CALI, using the photosensitizer KR, for targeted inactivation of AQP water transport in live cells. Various light inactivation strategies have been described previously, including dye-conjugated antibodies (Liao et al., 1994; Lamb et al., 1997), genetically encoded photosensitizers such as GFP (Rajfur et al., 2002; Vitriol et al., 2007), and a tetracysteine motif that binds biarsenical-fluorophore conjugates (Marek and Davis, 2002; Tour et al., 2003). KR was used here because of its approximately sevenfold greater CALI efficiency compared with GFP (Bulina et al., 2006), and because we were unable to obtain selective fluorescent biarsenical binding to tetracysteine motifs introduced in various extracellular loops in AQPs. Given the lack of nontoxic AQP inhibitors, spatially targeted inactivation of AQP water transport function provides an incisive tool for the study of AQP functions, such as cell migration, cell proliferation, and neural excitation.

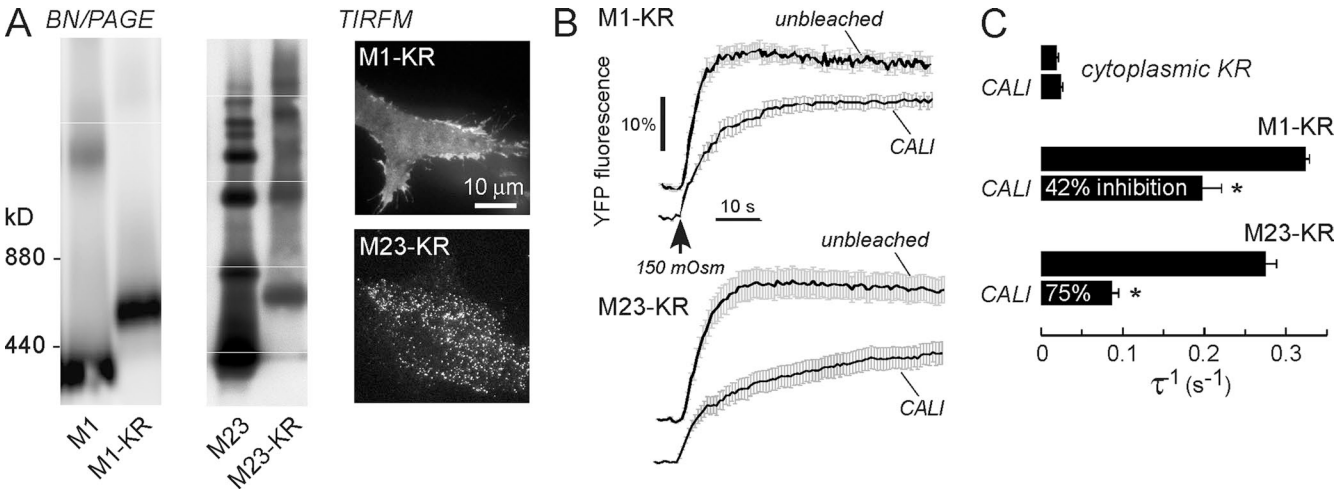

Figure 4. CALI efficiency depends on intermolecular topography. FRT cells were transfected with YFP alone or together with M1-AQP4-KR or M23-AQP4-KR. (A, left) AQP4 immunoblot after BN/PAGE. Gels that are apart were run separately. (A, right) TIRFM showing OAP formation by M23-AQP4-KR but not by M1-AQP4-KR. (B) Osmotic water permeability measured by YFP fluorescence, as in Fig. 3 B. (C) Relative osmotic water permeabilities (error bars indicate SE, $n = 5–8$ cells on three cover glasses; *, $P < 0.01$).

Our results provide evidence for both intramolecular and intermolecular CALI, as CALI efficiency depended on the length of the linker between AQP1 and KR, and on the intramembrane aggregation state of AQP4. CALI inactivation of M23-AQP4-KR caused disruption of myc-tagged M23-AQP4 coexpressed in intramembrane aggregates. Prior data indicate ROS production by the chromophore during CALI and presumed diffusion of ROS over 1–6 nm to inactivate the conjugated protein (Liao et al., 1994; Davies, 2003; Jacobson et al., 2008). Our data suggest that the ROS produced during CALI can inactivate nearby, but not covalently conjugated, proteins. As diagrammed in Fig. 6 C, ROS generated by a KR fluorophore affects proteins in a radius of 1–6 nm. In OAPs, where M23-AQP4-KR is clustered, ROS thus affects AQP4 molecules within some distance from the site of ROS production.

BN/PAGE analysis of AQP4 suggested that CALI produces intra- and intercellular cross-linking events and aggregation. Evidence for CALI-induced aggregate formation by SDS/PAGE was previously described for purified GST-GFP chimeras (McLean et al., 2009). It is thought that CALI results in the modification of specific amino acid side chains (histidine, tyrosine, tryptophan, methionine, or cysteine) by ROS (Davies, 2003), which leads to both intra- and intermolecular protein

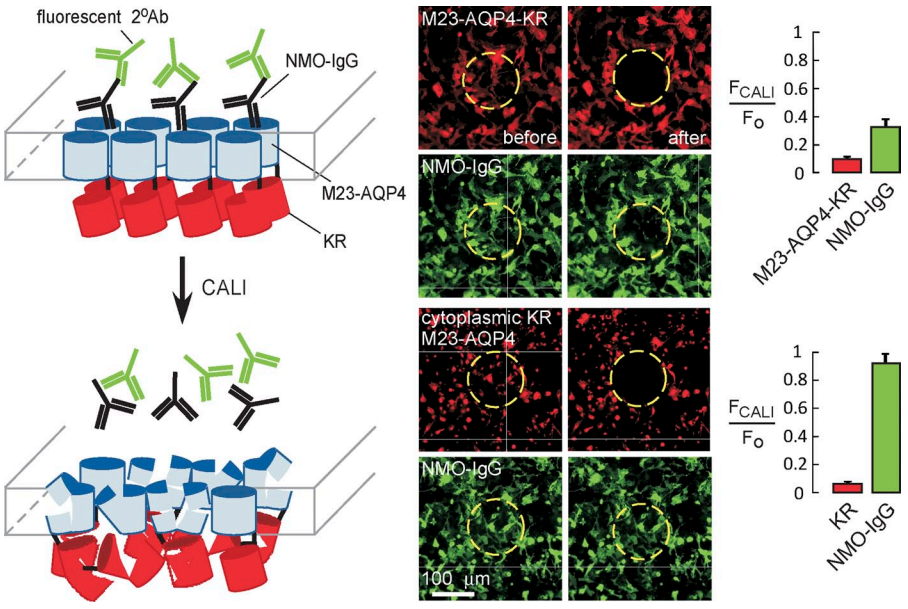

Figure 5. CALI reduces binding of NMO-IgG to an AQP4/KR chimera. (left) Schematic showing CALI of cells expressing M23-AQP4-KR and labeled with NMO-IgG and a secondary Alexa Fluor 488 anti–human antibody. (top middle) CALI (exposure to red light for 60 s) was performed in the indicated circles on cells expressing M23-AQP4-KR and labeled with NMO-IgG and a secondary Alexa Fluor 488 anti–human antibody. (bottom middle) CALI of control cells expressing cytoplasmic KR and unconjugated M23-AQP4. (right) Quantification of KR bleaching and loss of green Alexa Fluor 488 fluorescence after CALI ($n = 4$, error bars indicate SE; *, $P < 0.01$).

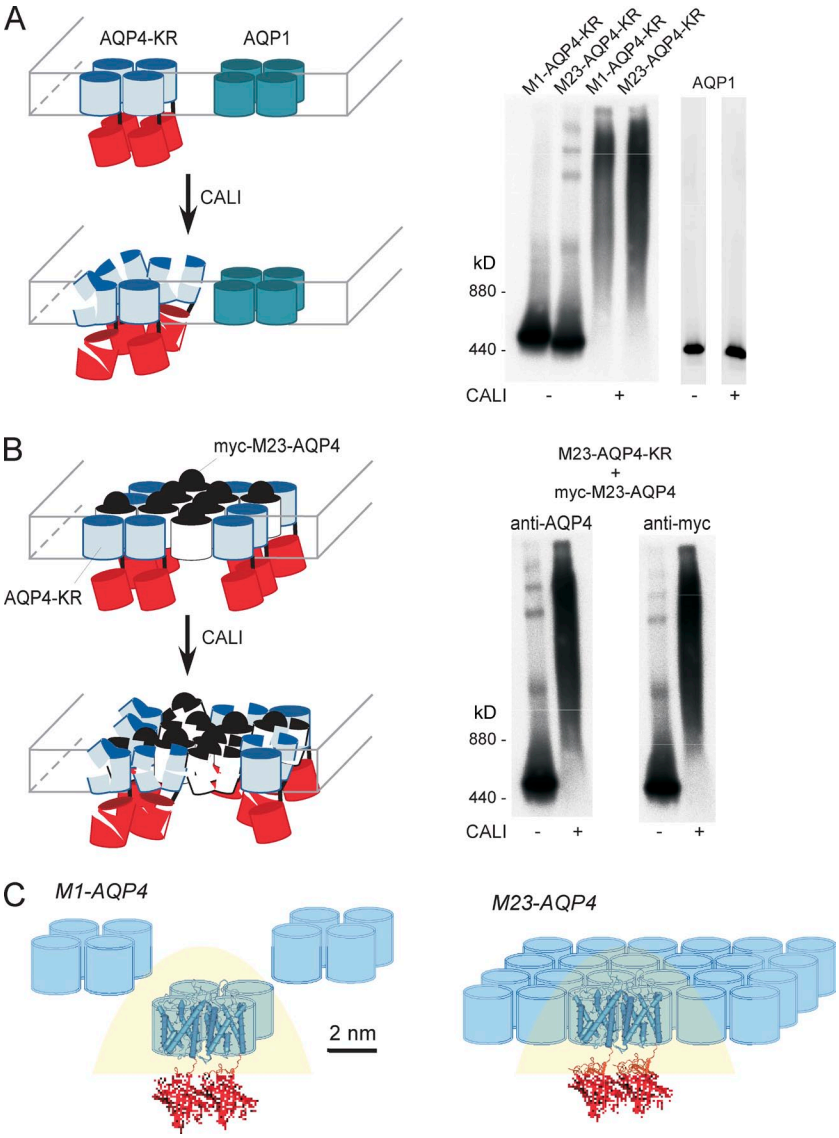

Figure 6. Intermolecular CALI in KR/AQP4 chimeras. (A, left) Schematic of cells expressing KR/AQP4 chimeras together with unconjugated AQP1. (A, right) AQP4 or AQP1 immunoblot after BN/PAGE of lysates from cells expressing M1-AQP4-KR or M23-AQP4-KR, together with unconjugated AQP1, with and without CALI. (B, left) Schematic of cells expressing M23-AQP4-KR together with myc-tagged M23-AQP4. (A, right) AQP4 and myc immunoblot of BN/PAGE of lysates from cells expressing M23-AQP4-KR together with myc-M23-AQP4, with and without CALI. Gels that are apart were run separately. (C) Schematic of distance and clustering-dependent CALI in M1-AQP4 and in OAP-forming M23-AQP4.

cross-linking, aggregation, and loss of activity. The global disruption of AQP structure likely accounts for CALI inhibition of AQP4 water transport and autoantibody binding.

In conclusion, we demonstrate the utility of KR for CALI of the AQPs 1 and 4. CALI produced rapid, spatially targeted, and irreversible inhibition of AQP water permeability as well as AQP-antibody association in live cells. Our results support the utility of KR to study the function and interactions of other membrane transporters and receptors, such as ion channels.

This work was supported by grants EB00415, DK35124, EY13574, HL73856, DK86125, and DK72517 from the National Institutes of Health and a grant from the Guthy-Jackson Charitable Foundation.

Edward N. Pugh served as editor.

Submitted: 26 August 2011
Accepted: 2 December 2011

REFERENCES

Bulina, M.E., D.M. Chudakov, O.V. Britanova, Y.G. Yanushevich, D.B. Staroverov, T.V. Chepurnykh, E.M. Merzlyak, M.A. Shkrob, S. Lukyanov, and K.A. Lukyanov. 2006. A genetically encoded photosensitizer. *Nat. Biotechnol.* 24:95–99. http://dx.doi.org/10.1038/nbt1175

Crane, J.M., and A.S. Verkman. 2008. Long-range nonanomalous diffusion of quantum dot-labeled aquaporin-1 water channels in the cell plasma membrane. *Biophys. J.* 94:702–713. http://dx.doi.org/10.1529/biophysj.107.115121

Crane, J.M., and A.S. Verkman. 2009. Determinants of aquaporin-4 assembly in orthogonal arrays revealed by live-cell single-molecule fluorescence imaging. *J. Cell Sci.* 122:813–821. http://dx.doi.org/10.1242/jcs.042341

Davies, M.J. 2003. Singlet oxygen-mediated damage to proteins and its consequences. *Biochem. Biophys. Res. Commun.* 305:761–770. http://dx.doi.org/10.1016/S0006-291X(03)00817-9

Del Bene, F., C. Wyart, E. Robles, A. Tran, L. Looger, E.K. Scott, E.Y. Isacoff, and H. Baier. 2010. Filtering of visual information in the tectum by an identified neural circuit. *Science.* 330:669–673. http://dx.doi.org/10.1126/science.1192949

Galietta, L.J., P.M. Haggie, and A.S. Verkman. 2001. Green fluorescent protein-based halide indicators with improved chloride and iodide affinities. *FEBS Lett.* 499:220–224. http://dx.doi.org/10.1016/S0014-5793(01)02561-3

Ho, J.D., R. Yeh, A. Sandstrom, I. Chorny, W.E. Harries, R.A. Robbins, L.J. Miercke, and R.M. Stroud. 2009. Crystal structure of human aquaporin 4 at 1.8 A and its mechanism of conductance. *Proc. Natl. Acad. Sci. USA.* 106:7437–7442. http://dx.doi.org/10.1073/pnas.0902725106

Huber, V.J., M. Tsujita, I.L. Kwee, and T. Nakada. 2009a. Inhibition of aquaporin 4 by antiepileptic drugs. *Bioorg. Med. Chem.* 17:418–424. http://dx.doi.org/10.1016/j.bmc.2007.12.038

Huber, V.J., M. Tsujita, and T. Nakada. 2009b. Identification of aquaporin 4 inhibitors using in vitro and in silico methods. *Bioorg. Med. Chem.* 17:411–417. http://dx.doi.org/10.1016/j.bmc.2007.12.040

Jacobson, K., Z. Rajfur, E. Vitriol, and K. Hahn. 2008. Chromophore-assisted laser inactivation in cell biology. *Trends Cell Biol.* 18:443–450. http://dx.doi.org/10.1016/j.tcb.2008.07.001

Jarius, S., and B. Wildemann. 2010. AQP4 antibodies in neuromyelitis optica: diagnostic and pathogenetic relevance. *Nat Rev Neurol.* 6:383–392. http://dx.doi.org/10.1038/nrneurol.2010.72

Lamb, R.F., B.W. Ozanne, C. Roy, L. McGarry, C. Stipp, P. Mangeat, and D.G. Jay. 1997. Essential functions of ezrin in maintenance of cell shape and lamellipodial extension in normal and transformed fibroblasts. *Curr. Biol.* 7:682–688. http://dx.doi.org/10.1016/S0960-9822(06)00295-8

Levin, M.H., P.M. Haggie, L. Vetrivel, and A.S. Verkman. 2001. Diffusion in the endoplasmic reticulum of an aquaporin-2 mutant causing human nephrogenic diabetes insipidus. *J. Biol. Chem.* 276:21331–21336. http://dx.doi.org/10.1074/jbc.M101901200

Liao, J.C., J. Roider, and D.G. Jay. 1994. Chromophore-assisted laser inactivation of proteins is mediated by the photogeneration of free radicals. *Proc. Natl. Acad. Sci. USA.* 91:2659–2663. http://dx.doi.org/10.1073/pnas.91.7.2659

Lu, M., M.D. Lee, B.L. Smith, J.S. Jung, P. Agre, M.A. Verdijk, G. Merkx, J.P. Rijss, and P.M. Deen. 1996. The human AQP4 gene: definition of the locus encoding two water channel polypeptides in brain. *Proc. Natl. Acad. Sci. USA.* 93:10908–10912. http://dx.doi.org/10.1073/pnas.93.20.10908

Ma, B., Y. Xiang, S.M. Mu, T. Li, H.M. Yu, and X.J. Li. 2004. Effects of acetazolamide and anordiol on osmotic water permeability in AQP1-cRNA injected *Xenopus* oocyte. *Acta Pharmacol. Sin.* 25:90–97.

Marek, K.W., and G.W. Davis. 2002. Transgenically encoded protein photoinactivation (FlAsH-FALI): acute inactivation of synaptotagmin I. *Neuron.* 36:805–813. http://dx.doi.org/10.1016/S0896-6273(02)01068-1

Maurel, C. 2007. Plant aquaporins: novel functions and regulation properties. *FEBS Lett.* 581:2227–2236. http://dx.doi.org/10.1016/j.febslet.2007.03.021

McLean, M.A., Z. Rajfur, Z. Chen, D. Humphrey, B. Yang, S.G. Sligar, and K. Jacobson. 2009. Mechanism of chromophore assisted laser inactivation employing fluorescent proteins. *Anal. Chem.* 81:1755–1761. http://dx.doi.org/10.1021/ac801663y

Monier, B., A. Pélissier-Monier, A.H. Brand, and B. Sanson. 2010. An actomyosin-based barrier inhibits cell mixing at compartmental boundaries in *Drosophila* embryos. *Nat. Cell Biol.* 12:60–65: 1–9. http://dx.doi.org/10.1038/ncb2005

Papadopoulos, M.C., S. Saadoun, and A.S. Verkman. 2008. Aquaporins and cell migration. *Pflugers Arch.* 456:693–700. http://dx.doi.org/10.1007/s00424-007-0357-5

Preston, G.M., J.S. Jung, W.B. Guggino, and P. Agre. 1993. The mercury-sensitive residue at cysteine 189 in the CHIP28 water channel. *J. Biol. Chem.* 268:17–20.

Rajfur, Z., P. Roy, C. Otey, L. Romer, and K. Jacobson. 2002. Dissecting the link between stress fibres and focal adhesions by CALI with EGFP fusion proteins. *Nat. Cell Biol.* 4:286–293. http://dx.doi.org/10.1038/ncb772

Rojek, A., J. Praetorius, J. Frøkiaer, S. Nielsen, and R.A. Fenton. 2008. A current view of the mammalian aquaglyceroporins. *Annu. Rev. Physiol.* 70:301–327. http://dx.doi.org/10.1146/annurev.physiol.70.113006.100452

Rossi, A., J.M. Crane, and A.S. Verkman. 2011. Aquaporin-4 Mz isoform: brain expression, supramolecular assembly and neuromyelitis optica antibody binding. *Glia.* 59:1056–1063. http://dx.doi.org/10.1002/glia.21177

Saadoun, S., M.C. Papadopoulos, M. Hara-Chikuma, and A.S. Verkman. 2005. Impairment of angiogenesis and cell migration by targeted aquaporin-1 gene disruption. *Nature.* 434:786–792. http://dx.doi.org/10.1038/nature03460

Serebrovskaya, E.O., T.V. Gorodnicheva, G.V. Ermakova, E.A. Solovieva, G.V. Sharonov, E.V. Zagaynova, D.M. Chudakov, S. Lukyanov, A.G. Zaraisky, and K.A. Lukyanov. 2011. Light-induced blockage of cell division with a chromatin-targeted phototoxic fluorescent protein. *Biochem. J.* 435:65–71. http://dx.doi.org/10.1042/BJ20101217

Shi, L.B., W.R. Skach, and A.S. Verkman. 1994. Functional independence of monomeric CHIP28 water channels revealed by expression of wild-type mutant heterodimers. *J. Biol. Chem.* 269:10417–10422.

Søgaard, R., and T. Zeuthen. 2008. Test of blockers of AQP1 water permeability by a high-resolution method: no effects of tetraethylammonium ions or acetazolamide. *Pflugers Arch.* 456:285–292. http://dx.doi.org/10.1007/s00424-007-0392-2

Soveral, G., C. Prista, T.F. Moura, and M.C. Loureiro-Dias. 2010. Yeast water channels: an overview of orthodox aquaporins. *Biol. Cell.* 103:35–54. http://dx.doi.org/10.1042/BC20100102

Tajima, M., J.M. Crane, and A.S. Verkman. 2010. Aquaporin-4 (AQP4) associations and array dynamics probed by photobleaching and single-molecule analysis of green fluorescent protein-AQP4 chimeras. *J. Biol. Chem.* 285:8163–8170. http://dx.doi.org/10.1074/jbc.M109.093948

Tour, O., R.M. Meijer, D.A. Zacharias, S.R. Adams, and R.Y. Tsien. 2003. Genetically targeted chromophore-assisted light inactivation. *Nat. Biotechnol.* 21:1505–1508. http://dx.doi.org/10.1038/nbt914

Umenishi, F., J.M. Verbavatz, and A.S. Verkman. 2000. cAMP regulated membrane diffusion of a green fluorescent protein-aquaporin 2 chimera. *Biophys. J.* 78:1024–1035. http://dx.doi.org/10.1016/S0006-3495(00)76661-6

Verbavatz, J.M., D. Brown, I. Sabolić, G. Valenti, D.A. Ausiello, A.N. Van Hoek, T. Ma, and A.S. Verkman. 1993. Tetrameric assembly of CHIP28 water channels in liposomes and cell membranes: a freeze-fracture study. *J. Cell Biol.* 123:605–618. http://dx.doi.org/10.1083/jcb.123.3.605

Verbavatz, J.M., T. Ma, R. Gobin, and A.S. Verkman. 1997. Absence of orthogonal arrays in kidney, brain and muscle from transgenic knockout mice lacking water channel aquaporin-4. *J. Cell Sci.* 110:2855–2860.

Verkman, A.S. 2008. Mammalian aquaporins: diverse physiological roles and potential clinical significance. *Expert Rev. Mol. Med.* 10:e13. http://dx.doi.org/10.1017/S1462399408000690

Vitriol, E.A., A.C. Uetrecht, F. Shen, K. Jacobson, and J.E. Bear. 2007. Enhanced EGFP-chromophore-assisted laser inactivation using deficient cells rescued with functional EGFP-fusion proteins. *Proc. Natl. Acad. Sci. USA.* 104:6702–6707. http://dx.doi.org/10.1073/pnas.0701801104

Walz, T., B.L. Smith, P. Agre, and A. Engel. 1994. The three-dimensional structure of human erythrocyte aquaporin CHIP. *EMBO J.* 13:2985–2993.

Walz, T., Y. Fujiyoshi, and A. Engel. 2009. The AQP structure and functional implications. *Handb. Exp. Pharmacol.* 190:31–56. http://dx.doi.org/10.1007/978-3-540-79885-9_2

Yang, B., T. Ma, and A.S. Verkman. 1995. cDNA cloning, gene organization, and chromosomal localization of a human mercurial insensitive water channel. Evidence for distinct transcriptional units. *J. Biol. Chem.* 270:22907–22913. http://dx.doi.org/10.1074/jbc.270.39.22907

Yang, B., D. Brown, and A.S. Verkman. 1996. The mercurial insensitive water channel (AQP-4) forms orthogonal arrays in stably transfected Chinese hamster ovary cells. *J. Biol. Chem.* 271:4577–4580. http://dx.doi.org/10.1074/jbc.271.9.4577

Yang, B., J.K. Kim, and A.S. Verkman. 2006. Comparative efficacy of HgCl2 with candidate aquaporin-1 inhibitors DMSO, gold, TEA+ and acetazolamide. *FEBS Lett.* 580:6679–6684. http://dx.doi.org/10.1016/j.febslet.2006.11.025

Yang, B., H. Zhang, and A.S. Verkman. 2008. Lack of aquaporin-4 water transport inhibition by antiepileptics and arylsulfonamides. *Bioorg. Med. Chem.* 16:7489–7493. http://dx.doi.org/10.1016/j.bmc.2008.06.005

Zhang, R., A.N. van Hoek, J. Biwersi, and A.S. Verkman. 1993. A point mutation at cysteine 189 blocks the water permeability of rat kidney water channel CHIP28k. *Biochemistry.* 32:2938–2941. http://dx.doi.org/10.1021/bi00063a002